order of magnitude larger than the longitudinal velocity perturbation. For a supersonic freestream, the maximum dust perturbation velocity is the same in both the longitudinal and in the transverse directions.

References

[1]Catalano, G. D., "Flow of a Marking Particle in a Two Dimensional Stagnation Region," Air Force Flight Dynamics Lab. Tech. Memo. No. 78-21, 1977.

[2]Liepman, H. W. and Roshko, A., "Small Perturbation Theory," *Elements of Gasdynamics*, Wiley, New York, 1957, pp. 202-215.

[3]Saffman, P. G., "The List on a Small Sphere in a Slow Shear Flow," *Journal of Fluid Mechanics*, Vol. 22, Pt. 2, June 1965, pp. 385-400.

Sullivan's Two-Celled Vortex

Fred W. Leslie* and John T. Snow†
Purdue University, West Lafayette, Ind.

IN Ref. 1, Sullivan presented an exact solution to the Navier-Stokes equations for a three-dimensional axisymmetric two-celled vortex. In the outer cell of this solution, fluid spirals inward from a large radius on stream surfaces that gradually turn upward from concentric cylindrical sheaths about the axis. Free-slip conditions are assumed on the lower surface with diffusive processes working only in the radial direction to balance the inward transport of angular momentum by the radial-axial velocity field. The inner cell consists of downward flow immediately about the axis. At the base of the vortex, this downward flow is turned outward and then moves upward with the swirling outer flow. Rotation within this cell is maintained by viscous diffusion.

In a cylindrical coordinate system, the radial, axial, and tangential velocity components and the pressure deficit are given by

$$u(r) = -ar + (6\nu/r)\,[1-\exp(-ar^2/2\nu)] \tag{1}$$

$$w(r,z) = 2az[1-3\exp(-ar^2/2\nu)] \tag{2}$$

$$v(r) = (\Gamma/2\pi r)\,[H(ar^2/2\nu)/H(\infty)] \tag{3}$$

$$\Delta p(r,z) \equiv p(r,z) - p(0,z) = -\frac{\rho}{2}\left\{4a^2z^2 + a^2r^2 + \frac{36\nu^2}{r^2}\left[1-\exp(ar^2/2\nu)\right]^2\right\} + \rho\int_0^r \frac{v^2}{r}\,dr \tag{4}$$

where a is the convergence strength of the flow-through field, ρ the fluid density (assumed constant), Γ the circulation at infinite radius, ν the kinematic viscosity, and H a function given by

$$H(x) = \int_0^x \exp\left\{-t + 3\int_0^t [(1-e^{-\tau})/\tau]\,d\tau\right\}dt \tag{5}$$

Received Dec. 10, 1979; revision received Feb. 19, 1980.

Index categories: Viscous Nonboundary-Layer Flows; Hydrodynamics.

*Postdoctoral Research Associate, Dept. of Geosciences.

†Assistant Professor, Dept. of Geosciences.

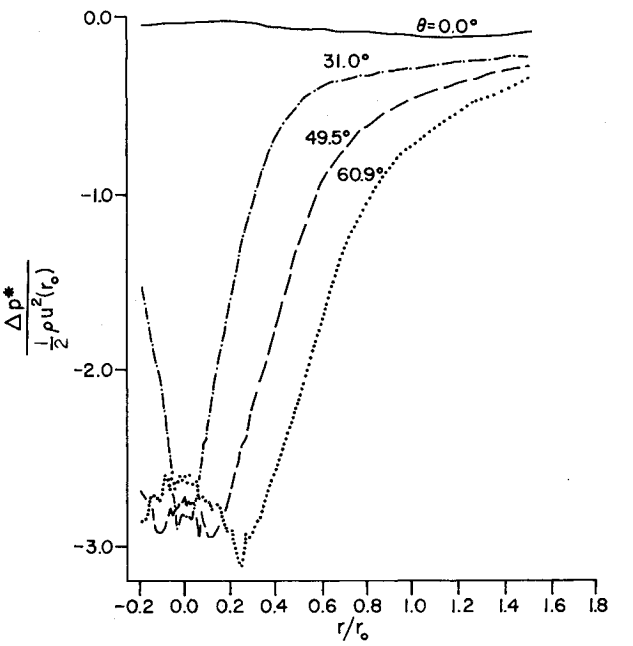

Fig. 1 Pressure profiles measured in the Purdue tornado simulator for various swirl angles.

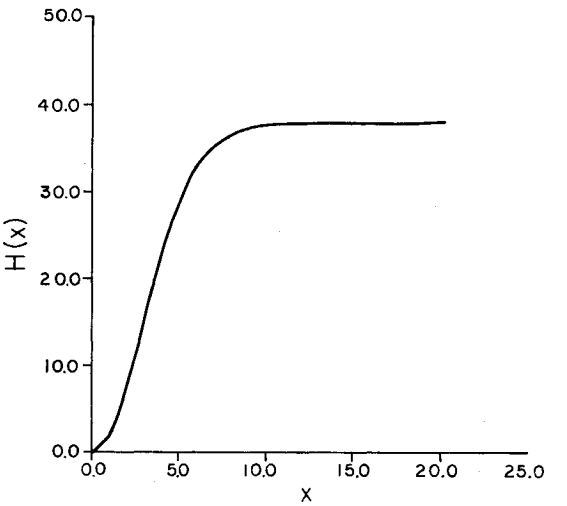

Fig. 2. $H(x)$ vs x, as given by Eq. (5).

Sullivan presented plots of the axial and tangential velocities as functions of radius, and compared the flow described by Eqs. 1-4 with the earlier parallel solution by Burgers[2,3] and Rott[4,5] for a one-celled vortex. Here, Sullivan's note is extended by providing a tabulation of $H(x)$, by evaluating Eq. (5), and by presenting plots of the surface pressure deficit. This work was motivated by recent measurements by the authors[6,7] of the wall static pressure fields beneath two-celled vortices generated in laboratory tornado simulators.

In order to better understand the behavior of the vortex core pressure, it is more informative to measure $p(r,0) - p(r_{ref},0) \equiv \Delta p^*(r)$ (where r_{ref} is a reference radius in the far-field of the flow) than Sullivan's $\Delta p(r) = p(r,0) - p(0,0)$. These two different representations of pressure deficit differ only by the amount $p(0,0) - p(r_{ref},0)$. A set of radial pressure profiles measured in the Purdue tornado simulator is shown in Fig. 1. The radial position is nondimensionalized by r_0, a characteristic radial scale of the apparatus. Similarly, the pressure deficit is nondimensionalized by $1/2\ \rho u^2(r_0)$. The profiles were measured for a fixed geometry and volume flow rate. Each profile in the set is characterized by a selected value of far-field angular momentum. This is indicated by the given

Table 1 Values of $H(x)/H(\infty)$

x	$H(x)/H(\infty)$	x	$H(x)/H(\infty)$	x	$H(x)/H(\infty)$
0.00	0.0	6.40	8.9361E−01	12.80	9.9891E−01
0.20	6.4192E−03	6.60	9.0593E−01	13.00	9.9906E−01
0.40	1.5464E−02	6.80	9.1698E−01	13.20	9.9920E−01
0.60	2.7598E−02	7.00	9.2686E−01	13.40	9.9932E−01
0.80	4.3191E−02	7.20	9.3567E−01	13.60	9.9942E−01
1.00	6.2481E−02	7.40	9.4351E−01	13.80	9.9950E−01
1.20	8.5554E−02	7.60	9.5047E−01	14.00	9.9958E−01
1.40	1.1234E−01	7.80	9.5664E−01	14.20	9.9964E−01
1.60	1.4263E−01	8.00	9.6209E−01	14.40	9.9970E−01
1.80	1.7609E−01	8.20	9.6691E−01	14.60	9.9974E−01
2.00	2.1227E−01	8.40	9.7115E−01	14.80	9.9978E−01
2.20	2.5066E−01	8.60	9.7487E−01	15.00	9.9982E−01
2.40	2.9073E−01	8.80	9.7815E−01	15.20	9.9984E−01
2.60	3.3191E−01	9.00	9.8102E−01	15.40	9.9987E−01
2.80	3.7366E−01	9.20	9.8353E−01	15.60	9.9989E−01
3.00	4.1547E−01	9.40	9.8572E−01	15.80	9.9991E−01
3.20	4.5686E−01	9.60	9.8764E−01	16.00	9.9992E−01
3.40	4.9743E−01	9.80	9.8931E−01	16.20	9.9994E−01
3.60	5.3684E−01	10.00	9.9076E−01	16.40	9.9995E−01
3.80	5.7477E−01	10.20	9.9202E−01	16.60	9.9996E−01
4.00	6.1102E−01	10.40	9.9312E−01	16.80	9.9996E−01
4.20	6.4541E−01	10.60	9.9407E−01	17.00	9.9997E−01
4.40	6.7783E−01	10.80	9.9490E−01	17.20	9.9998E−01
4.60	7.0819E−01	11.00	9.9561E−01	17.40	9.9998E−01
4.80	7.3648E−01	11.20	9.9623E−01	17.60	9.9998E−01
5.00	7.6270E−01	11.40	9.9676E−01	17.80	9.9999E−01
5.20	7.8689E−01	11.60	9.9722E−01	18.00	9.9999E−01
5.40	8.0910E−01	11.80	9.9761E−01	18.20	9.9999E−01
5.60	8.2941E−01	12.00	9.9796E−01	18.40	1.0000E+00
5.80	8.4792E−01	12.20	9.9825E−01	18.60	1.0000E+00
6.00	8.6471E−01	12.40	9.9850E−01	18.80	1.0000E+00
6.20	8.7991E−01	12.60	9.9871E−01	19.00	1.0000E+00

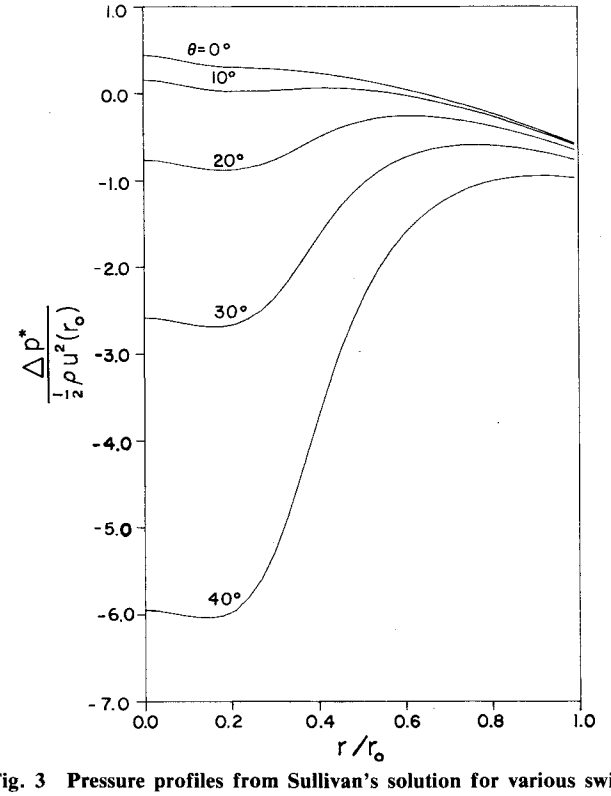

Fig. 3 Pressure profiles from Sullivan's solution for various swirl angles.

values of the swirl angle θ, where $\theta=\tan^{-1}[v(r_0)/u(r_0)]$. These reference velocities were measured with a hot-film anemometer. The primary feature to be noted is the prominent off-axis pressure minimum for large values of the swirl angle.

For comparison of the observed profiles with Sullivan's solution, values of $H(x)$ were computed numerically using Simpson's second rule. As shown in Fig. 2, this function is essentially constant for large arguments, then decreases rapidly to zero for smaller values of x. When normalized by its asymptotic value ($H(\infty)=37.905$), $H(x)$ represents the fraction of far-field angular momentum conserved as the flow spirals inward. Table 1 lists values of $H(x)/H(\infty)$. Clearly, $H(x)$ is practically constant for arguments greater than about 15.

The value of a was determined from the imposed volume flow rate, and the ambient circulation was computed from the corresponding radial inflow and the specified swirl angle at r_0. Choosing an appropriate value of viscosity was not straightforward. Using the molecular value resulted in core sizes which were much smaller than observed in the laboratory. Instead, the value was chosen so as to produce a specified core radius r_c. For $r_c/r_0=0.4$, $\nu=7\times10^{-3}\text{m}^2\text{s}^{-1}$. Laboratory observations indicate that if the geometry and flow rate are fixed, the vortex core expands with increasing swirl angle. However, in order to simplify interpreting the effect of increasing only the ambient swirl on the shape of the profiles, the curves in Fig. 3 were computed with the core radius fixed at $r_c/r_0=0.4$. It should be pointed out that the pressure profiles are very sensitive to the core radius selected. If a small core is taken, the tangential velocity is much higher, creating a larger central pressure drop. In fact, for a sufficiently small core, the contribution to the pressure from the central downdraft is completely masked so that the pressure decreases all the way to the axis.

The pressure profiles computed from Sullivan's model are shown in Fig. 3 for various swirl angles and are nondimensionalized as in Fig. 1. The value of the pressure deficit at $r/r_0=1$ was determined by matching the Sullivan solution to a simple potential flow solution which simply conserves mass and angular momentum through the inlet channel of the apparatus. The curves for $\theta=30$ and 40 deg in Fig. 3 show

qualitatively many of the features seen in the measured profiles. Foremost is the off-axis pressure minimum. A progressive decrease in pressure in the interval $0.25 \leq r/r_0 \leq 1.0$ is also noted. The discrepancy in the magnitude of the central pressure drop is partially due to the use of a fixed core radius. It should be mentioned that the positive values of $\Delta p^*/\frac{1}{2}\rho u^2(r_0)$ for small r and θ result from the fact that $\Delta p(0,0)=0$ and that $p(0,0)-p(r_{\text{ref}},0)$ is positive for small r and θ.

Several deficiencies in Sullivan's solution should be noted. Most importantly, there is no coupling between v and the u,w field. This is due to the assumption of the forms of u and w at the outset, and then solving the tangential momentum equation to find a consistent v field, all subject to a free-slip condition on the lower surface. The u, w field has unrealistic far-field conditions since $u(r)\to\infty$ as $r\to\infty$, and $w(r,z)\to\infty$ as $z\to\infty$. The free-slip condition eliminates endwall boundary-layer effects, which are known to be important in swirling flows. As a consequence of this lack of coupling between the tangential and flow-through fields, the model is limited in its ability to properly respond to changes in background conditions (e.g., the radius of maximum tangential velocity is a constant independent of both the height z and the far-field circulation Γ; further, the intensity of the downflow along the centerline is independent of Γ). Also, the viscosity ν is taken to be constant throughout the volume. While this is a good assumption for laminar vortices, recent work by Lewellen and Teske[8] has shown that use of a constant "eddy" viscosity value to model turbulent vortices is not a valid approach.

These considerations limit the usefulness of Eq. (4) in modeling the experimentally observed pressure profiles. While good fits to the profiles in Fig. 1 could be obtained by selecting a different value of ν for each value of Γ (a being held fixed), the physical justification for doing so is not clear. However, in conclusion, it is noted that Sullivan's solution does appear to incorporate some of the essential physics of actual two-celled vortices. In particular, the role of the downdraft along the centerline in creating the central pressure hump is well brought out. Also, the overall progression of the shape of the radial profile of the wall static pressure on the lower surface as the input angular momentum is increased is also qualitatively reproduced.

References

[1] Sullivan, R.D., "A Two-Cell Vortex Solution of the Navier-Stokes Equation," *Journal of the Aerospace Sciences*, Vol. 26, No. 11, Nov. 1959, pp. 767-768.

[2] Burgers, J. M., "Application of a Model System to Illustrate Some Points of the Statistical Theory of Free Turbulence," *Proceedings of the Academy of Sciences, Amsterdam*, Vol. 43, No. 1, 1940, pp. 2-12.

[3] Burger, J. M., "A Mathematical Model Illustrating the Theory of Turbulence," *Advances in Applied Mechanics*, Vol. 1, Academic Press, New York, 1948, pp. 197-199.

[4] Rott, N., "On the Viscous Core of a Line Vortex," *ZAMP*, Vol. 9b, No. 5/6, March 1958, pp. 543-553.

[5] Rott, N., "On the Viscous Core of a Line Vortex II," *ZAMP*, Vol. 10, No. 1, Jan. 1959, pp. 73-81.

[6] Leslie, F. W., "The Dependence of the Maximum Tangential Velocity on Swirl Ratio in a Laboratory Simulator," *Preprints of the 11th Conference on Severe Local Storms*, American Meterological Society, Kansas City, Mo., Oct. 1979, pp. 361-366.

[7] Snow, J. T., Church, C.R., and Barnhart, B. J., "An Investigation of the Surface Pressure Fields beneath Simulated Tornado Cyclones," *Preprints of the 11th Conference on Severe Local Storms*, American Meteorological Society, Kansas City, Mo., Oct. 1979, pp. 367-374.

[8] Lewellen, W. S. and Teske, M. E., "Turbulent Transport Model of Low-Level Winds in a Tornado," *Preprints of the 10th Conference on Severe Local Storms*, American Meteorological Society, Omaha, Neb., Oct. 1977, pp. 291-298.

J80-244

80006

Stiffness Matrix Correction from Incomplete Test Data

Fu-Shang Wei*

Kaman Aerospace Corporation, Bloomfield, Conn.

Nomenclature

d	= weighted norm of the errors between the given and the optimal stiffness matrix
I	= unity matrix
K	= stiffness matrix
k_{ij}	= ij element of K
M	= mass matrix
m_{ij}	= ij element of M
Y	= optimal stiffness matrix
y_{ij}	= ij element of Y
Z	= general-coordinates vector
Φ	= orthogonal mode shape matrix
Φ_{ij}	= ij element of Φ
ψ	= Lagrange function for stiffness matrix
β_y	= matrix of Lagrange multiplier
$\beta_{y,ij}$	= ij element of β_y
Λ_y	= matrix of Lagrange multiplier
$\lambda_{y,ij}$	= ij element of Λ_y
Ω^2	= measured frequency matrix
ω_{ij}^2	= ij element of Ω^2
$(\ )^T$	= transpose of ( )

Introduction

IN Refs. 1 and 2, Baruch and Bar-Itzhack use the Lagrange multiplier method to optimally correct the stiffness matrix from test data. The resulting stiffness matrix which satisfies the dynamic equation is symmetric. However, the Lagrange multiplier Λ_y, which is used to define the Lagrange function ψ, is difficult to obtain without making any assumption. The crucial assumption for the matrix $\Lambda_y^T MX$, which is assumed to be symmetric in Ref. 2, is not always true in general and is hard to understand from a physical point of view. The main purpose of this Technical Note is to propose a new approach which shows the uniqueness of the corrected stiffness matrix in a different way than that given in Ref. 2. The corrected stiffness matrix Y can be directly obtained without making any assumptions. It is very interesting that by algebraic manipulation the Lagrange multiplier Λ_y can be eliminated from the derivation. Thus, the necessity to calculate Λ_y can be avoided.

Optimization Procedure for Correcting the Stiffness Matrix

In an incomplete test, the measured modal matrix $\Phi(n\times m)$ is rectangular, where $n \geq m$, and the mass matrix $M(n\times n)$ is a positive-definite symmetric matrix. The mode shapes and mass matrix must be orthogonal to fulfill the basic requirement before starting to correct the stiffness matrix.

$$\Phi^T M\Phi = I \tag{1}$$

Following Refs. 1 and 2, the simplest way to find a symmetric stiffness matrix Y, which is closest to the measured or computed stiffness matrix K, is given by minimizing the norm

Received Oct. 15, 1979.

Index category: Structural Dynamics.

*Research Engineer Specialist. Member AIAA.